



Contents lists available at ScienceDirect

## Arabian Journal of Chemistry

journal homepage: [www.ksu.edu.sa](http://www.ksu.edu.sa)

Original article

Electrochemical sensing of gatifloxacin using Ag<sub>2</sub>S/RGO nanocomposite

Chunxia Yao<sup>a,b,c,1</sup>, Ying Liang<sup>d,1</sup>, Sai Huang<sup>a,e</sup>, Chengbin Liu<sup>a,b,c,\*</sup>,  
Wei Song<sup>a,b,c,\*</sup>, Weiguo Song<sup>a,b,c,\*</sup>

<sup>a</sup> The Institute of Agro-food Standards and Testing Technology, Shanghai Academy of Agricultural Sciences, Shanghai 201403, China

<sup>b</sup> Key Laboratory of Food Quality Safety and Nutrition (Co-construction by Ministry and Province), Ministry of Agriculture and Rural Affairs, Shanghai 201403, China

<sup>c</sup> Shanghai Engineering Research Center for Agri-product Quality and Safety, Shanghai 201403, China

<sup>d</sup> School of Pharmacy, Shanghai University of Medicine and Health Sciences, Shanghai 201318, China

<sup>e</sup> School of Materials Science and Engineering, Shanghai Institute of Technology, 100 Haiquan Road, Shanghai 201418, China

## ARTICLE INFO

## Keywords:

Silver sulfide  
Reduced graphene oxide  
Electrochemical sensor  
Gatifloxacin  
Real sample

## ABSTRACT

As a widely-used fluoroquinolone antibiotics, 1-Cyclopropyl-6-fluoro-8-methoxy-7-(3-methyl-1-piperazinyl)-4-oxo-1,4-dihydro-3-quinolinecarboxylic acid (gatifloxacin, GAT) has aroused much concern recently and it is of great importance to realize the accurate and efficient detection. Herein, the silver sulfide/reduced graphene oxide composite (Ag<sub>2</sub>S/RGO) was synthesized with one-pot method and was coated on the glassy carbon electrode to develop an effective electrochemical sensor for GAT. After the optimization of the size of Ag<sub>2</sub>S, the pH of buffer solution, and the scanning rate, the Ag<sub>2</sub>S/RGO modified electrode exhibits good linear relationship to GAT within wide ranges of 0.2 μM – 20 μM and 20 μM – 250 μM with a detection limit of 0.0667 μM. Besides, the proposed sensor shows good selectivity to GAT versus multiple interferences, including organic compounds, ions, and other antibiotics. At last, the proposed sensor was successfully applied in the GAT analysis in various real samples (including shrimp, fish, and chicken) with satisfying recoveries of 91.8 % – 102.4 %. In general, the proposed Ag<sub>2</sub>S/RGO-based electrochemical sensor provides a novel strategy for the GAT analysis, which is of significance for the development of efficient analytical techniques for antibiotics.

## 1. Introduction

Gatifloxacin (GAT) belongs to the fourth generation of fluoroquinolones. It has a wide antibacterial spectrum and strong antibacterial property, which is widely employed in aquaculture and animal husbandry. After entering the human body through the food chain, excessive gatifloxacin may cause severe threat to human health (Wan et al., 2023). Therefore, it is of great significance to analyze the accurate concentration of gatifloxacin (Ji et al., 2024; Van Doorslaer et al., 2014; Speltini et al., 2015). At present, the quantitative analytical methods of fluoroquinolones mainly include capillary electrophoresis (Tian et al., 2014), ultraviolet spectrophotometry (Darwish et al., 2010), fluorescence spectrophotometry (Vosough et al., 2015), and high performance liquid chromatography (Storey et al., 2014; Meng et al., 2015). However, these methods often have high dependence on large instruments and professional operators, which are inconvenient and have high cost. Compared with the above-mentioned methods, electrochemical sensor has the advantages of low cost, fast response, simple equipment, high

sensitivity, and good reliability, which is convenient for the rapid detection of trace chemicals (Mo et al., 2024; Keziban., 2022; Abd El-Rahman et al., 2021; Santos et al., 2021; Wang et al., 2023). For example, Huang et al. (2023) fabricated a molecularly imprinted electrochemical sensor for the selective determination of gatifloxacin based on multi-walled carbon nanotube (MWCNT), zeolitic imidazolate framework 8 (ZIF-8), and dual functional monomers (Huang et al., 2023). For electrochemical sensors, the electrode modification materials are the central part, which, to a large extent, determines the analytical performance of the sensors. Therefore, in order to further improve the detection efficiency, it is necessary to find materials with superior conductivity and large specific surface area for electrode modification.

In recent years, explorations about the preparation, properties, and applications of semiconductor nanoparticles have been investigated in electrochemical sensors (Kang et al., 2015; Liang et al., 2019). Graphene has a two-dimensional structure with a single layer of closely arranged carbon atoms, which has good conductivity (Karuppasamy et al., 2022; Venkatesh et al., 2022), high stability (Lahcen et al., 2020; Keziban,

\* Corresponding authors.

E-mail addresses: [liuchengbin@saas.sh.cn](mailto:liuchengbin@saas.sh.cn) (C. Liu), [songwei890214@163.com](mailto:songwei890214@163.com) (W. Song), [songweiguo@saas.sh.cn](mailto:songweiguo@saas.sh.cn) (W. Song).

<sup>1</sup> Chunxia Yao and Ying Liang: These authors contributed equally to the manuscript.

<https://doi.org/10.1016/j.arabjc.2024.106031>

Received 12 April 2024; Accepted 17 October 2024

Available online 20 October 2024

1878-5352/© 2024 The Author(s). Published by Elsevier B.V. on behalf of King Saud University. This is an open access article under the CC BY-NC-ND license (<http://creativecommons.org/licenses/by-nc-nd/4.0/>).

2019), large specific surface area (Bo et al., 2017) and good biocompatibility (Akkarachchainon et al., 2017; Wu et al., 2019). In order to improve the conductivity of electrode materials, graphene with special band structure could be a good choice and has been widely applied in the construction of electrochemical sensors (Neslihan et al., 2020; Vlassioux et al., 2015; Thangavelu et al., 2017; Chekin et al., 2018; Chekin et al., 2019; Ladmakhi et al., 2020). For example, Mao et al. (2012) fabricated an immunosensor using graphene sheet-methylene blue (GS-MB) nanocomposites for the detection of prostate-specific antigen (PSA) as a model analyt (Mao et al., 2012). The sensor showed a linear range of 0.05–5.00 ng/mL and a detection limit of 13 pg/mL due to the efficient adsorption of antibodies on MB and the improved electroactivity of MB in the presence of graphene. In another work, the use of MnO<sub>2</sub>/GO composites was developed for hydrazine detection (Singh et al., 2023). The composites exhibited a high electrochemical sensing performance with a linear range of 3 μM to 1.12 mM, a detection limit of 0.16 μM, and a sensitivity of 1.007 mA mM<sup>-1</sup> cm<sup>-2</sup>. This performance can be attributed to the oxygen-containing groups and large specific surface area of GO, which provide excellent adsorption properties for the consequent hydrazine.

Silver sulfide (Ag<sub>2</sub>S) is a highly chemical-stable semiconductor material and an important electronic functional material (Tang et al., 2024; Li et al., 2020; Chen et al., 2014; Khadija et al., 2023; Keziban et al., 2023; Aydın et al., 2024), which has been widely used in photovoltaic cells, superconductors, photoconductors, infrared detection, electrochemical sensors, and other fields due to its good photoelectric performance, biocompatibility, and low toxicity (Lu et al., 2018; Mazurkóv et al., 2022; Wu et al., 2018). For example, Cai et al. (2019) prepared Ag<sub>2</sub>S-modified calcein electrode by fluorescence ratio method, which can detect ALP in human serum with low detection limit (Cai et al., 2019). Moreover, silver sulfide nanoparticles have large specific surface area and good dispersion (Chen et al., 2021), which can be put into use as excellent electrode materials. Therefore, silver sulfide shows promise as a superior material to modify RGO and it is of great potential to develop a novel electrochemical sensor for GAT based on Ag<sub>2</sub>S/RGO composites.

In this work, silver sulfide/reduced graphene oxide composites (Ag<sub>2</sub>S/RGO) were synthesized with one-step method. Then, the particle size and experimental conditions were optimized for the modification of electrode to realize the electrochemical sensing of GAT as illustrated in

Scheme 1. The atomic structure, morphology, and electrochemical behavior of the materials were characterized and studied by X-ray diffraction (XRD), transmission electron microscopy (TEM), scanning electron microscopy (SEM), and electrochemical methods. The prepared Ag<sub>2</sub>S/RGO modified electrode shows an excellent sensing performance for gatifloxacin, including high sensitivity, low detection limit, good stability, and satisfactory reproducibility. These results demonstrate that the Ag<sub>2</sub>S/RGO composites shows improved electrochemical properties and the newly-developed electrochemical sensor has an excellent potential in the practical applications of antibiotic analysis in the environment.

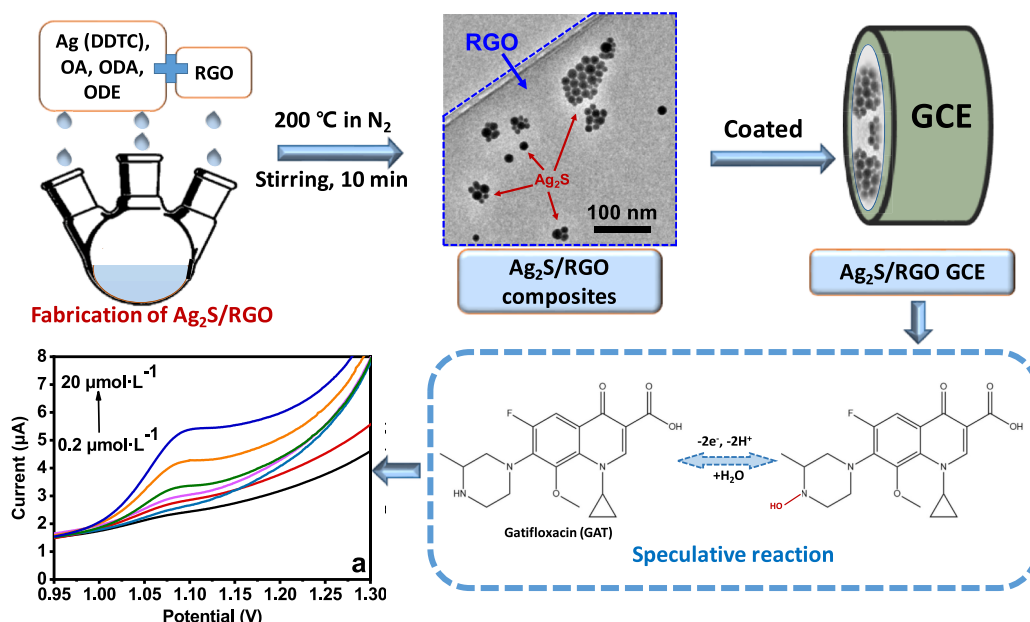
## 2. Experimental section

### 2.1. Materials and reagents

Gatifloxacin hydrochloride, reduced graphene oxide (RGO), silver diethyldithiocarbamate (Ag (DDTC)), oleic acid (OA, 90 %), octadecylamine (ODA, 90 %), 1-octadecene (ODE, 90 %), and N, N-dimethylformamide (DMF, 99 %) are purchased from Sigma-Aldrich company (Merck, Darmstadt, Germany) without further purification. Potassium dihydrogen phosphate, purchased from Sinopharm Group Co., Ltd. (Beijing, China), is used to prepare 0.1 mol·L<sup>-1</sup> phosphate buffer solution (PBS buffer). Ultra-pure water (Millipore, Merck, Darmstadt, Germany) was used throughout the experiments, and all experiments are carried out at room temperature.

### 2.2. Material synthesis and sensor preparation

0.1 mmol/L of Ag (DDTC), 10 mmol/L of OA, 10 mmol/L of ODA, and 20 mmol/L of ODE were added to a 100 mL three-necked flask as a solvent. To remove any water and oxygen, the solution was continuously stirred and heated to 100°C until it became transparent. The solution was heated to 200°C (with a heating rate of 15 °C/min) and kept in N<sub>2</sub> atmosphere for 10 min, 25 min, and 45 min. After cooling to room temperature, add excessive ethanol into the reaction solution. Then, wash and centrifuge the solution at 12000 rpm for 10 min. Repeat the above operation for 5 times, and finally dry the solid in air at 60°C. The resulting nanocrystals are easily redistributed in nonpolar organic solvents, i.e., cyclohexane. The yield of nano-crystalline is about 60–70 %



Scheme 1. The scheme of the fabrication of Ag<sub>2</sub>S/RGO composites and its electrochemical sensing application for gatifloxacin (GAT).

(Du et al., 2010). In addition, the synthesis of Ag<sub>2</sub>S/RGO is the same as that of Ag<sub>2</sub>S, except that 1 mg of RGO dissolved in 1 mL DMF is added to the three neck flask, and the reaction time is 10 min.

The bare glassy carbon electrode (GCE) was polished with alumina powder (0.1 μm) and alumina powder (0.05 μm) successively, then washed with deionized water twice, washed with ethanol for 1 min, and dried and cooled for use. A certain amount of Ag<sub>2</sub>S or Ag<sub>2</sub>S/RGO (2 mg) was mixed with 50 μL chitosan (1 mg/mL) and 80 μL chloroform, and then 4.0 μL of the mixed solution with Ag<sub>2</sub>S/RGO nanocomposites was dropped on the surface of the treated GCE. The brief diagram for the fabrication process of Ag<sub>2</sub>S/RGO composites was illustrated in Scheme 1. After drying, the modified electrode was washed thoroughly with secondary distilled water. When not in use, grind and polish the modified electrode with alumina powder in turn, immerse it in PBS (pH 7.0, 0.1 mol/L), and keep it at constant temperature of 4 °C, which can make the reaction liquid junction be moist and smooth and is very helpful for the modified electrode potential to maintain stable.

### 2.3. Instrument analysis

The electrochemical experiments were carried out on a CHI 660E electrochemical workstation (Chinstruments, Shanghai, China) (Yao et al., 2024). The SEM images were recorded with a Regulus 8100 (Hitachi, Tokyo, Japan), and the energy dispersive spectrometer (EDS) spectra were obtained with an EDAX EDS Element (AMETEK Inc., Berwyn, USA). XRD results was measured with a D/max-2600PC (Rigaku Corporation, Tokyo, Japan) via ceramic-monochromatic Cu K, which was operated at 45 kV and 20 mA with a scanning range of 20–70° and a scanning rate of 5°/min in 2θ. The transmission electron microscopy (TEM) was performed on a Talos F200S (FEI 2 SDD, Thermo Scientific, USA).

### 2.4. Electrochemical detection

Linear Sweep Voltammetry (LSV) is a common electrochemical analytical technique with three electrodes that studies the redox behavior of electroactive species in solution by applying a linearly varying voltage (sweep voltage) to the working electrode and measuring the resulting current. Moreover, LSV method has the advantages of simple operation, high sensitivity, and wide application range, and has been widely used in analytical chemistry, materials science, biochemistry, environmental science and other fields. The kinetic parameters of the reaction can be determined by analyzing the slope and shape of the current–potential curve. Therefore, in this work, LSV analysis with a typical three-electrode cell, including a platinum wire as the auxiliary electrode, a modified GCE as the working electrode (glassy carbon disk electrode with 3 mm diameter and 7.065 mm<sup>2</sup> geometric area), and a saturated calomel electrode (SCE) as the reference electrode, was applied to detect GAT. The optimization of pH was carried out with the addition of acetate in the PBS buffer. When performing the electrochemical testing, the modified electrodes were first placed in acetate buffer (pH = 4.0) containing different concentrations of GAT and then deposited using the current–time method to achieve electrodeposition. After stirring and letting stand, the dissolution peak of GAT was recorded via oxidative dissolution measurements with LSV, in which the step increments is 4 mV, and the scanning potential range is –1.0 to –0.2 V. After each test, the potential was returned to 0.1 V and the electrodes were washed for 120 s for clean-up. In the anti-interference and stability experiments, the same conditions were carried out. Besides, the CV measurements were carried out in a mixture solution of 20 mmol·L<sup>-1</sup> K<sub>3</sub>[Fe(CN)<sub>6</sub>]/K<sub>4</sub>[Fe(CN)<sub>6</sub>] and 0.1 mol·L<sup>-1</sup> KCl with a scan rate of 100 mV·s<sup>-1</sup>. Three kinds of real samples, including shrimp, crucian carp, chicken meat, were collected from Shanghai market. The pretreatment was based on the standard method as reported before (GB/T 20366–2006). 5.0 g of sample, 20 mL of formic acid-acetonitrile solution were added to a 50 ml polyfluoroethylene centrifuge tube. Then,

centrifuge the solution at 4000 rpm for 5 min. In simple terms, the sample is placed in a petri dish and different concentrations of gatifloxacin are added to the sample. The samples were stored at 4 °C and tested with Ag<sub>2</sub>S/RGO electrochemical sensors. Before the analysis of GAT, the pH of extracted samples was modified to 4.0 using acetate buffer solution. The concentrations of GAT in the real samples was fabricated with the standard addition method (10, 100, and 200 μmol·L<sup>-1</sup>), and then LSV analysis was carried out for three parallels.

## 3. Results and discussion

### 3.1. Material characterization

X-ray diffraction (XRD), transmission electron microscopy (TEM), and scanning electron microscopy-x-ray energy dispersive spectrometer (SEM-EDS) were used to characterize the crystal phase, morphology, structure and element content of the materials. Ag<sub>2</sub>S was synthesized in the organic phase of diethyldithiocarbamate (Ag (DDTC)), oleic acid (OA), octadecylamine (ODA) and 1-octadecene (ODE). Ag<sub>2</sub>S nanoparticles with different particle size were prepared by controlling the reaction time. X-ray diffraction (XRD) was applied to determine and analyze the crystal structure of the synthetic Ag<sub>2</sub>S nanoparticles. The results in Fig. S1 (Supplementary Material) indicate that the material prepared by organic phase method is monoclinic Ag<sub>2</sub>S because of the similar pattern of the synthesized materials to the standard JCPDS 14–0072 (Jang et al., 2021). In details, the angle, height and shape of the corresponding peaks in the two patterns are basically the same, and the characteristic diffraction peaks (28.97°, 31.52°, 34.39°, 40.74°) generally coincide (Ghayeb et al., 2016).

Based on the XRD data of Ag<sub>2</sub>S and Scherrer formula, Ag<sub>2</sub>S particle size with a reaction time of 10 min can be estimated to be 13.6 nm.

$$D = \frac{K\lambda}{\beta\cos\theta} = \frac{0.89 \times 0.15405}{\frac{0.60}{180} \times \pi \times \cos(\frac{31.52}{2})} = 13.6\text{nm}$$

As shown in Fig. S1, the XRD spectra of the fabricated Ag<sub>2</sub>S is well consistent with the Ag<sub>2</sub>S standard card, indicating the successful synthesis of Ag<sub>2</sub>S. Besides, the successful fabrication of Ag<sub>2</sub>S can also be proved by the EDS results in Fig. S2, in which the Ag peak is clearly observed. As shown in Fig. S2 and Table S1 in the Supplementary Material, the Scanning electron microscope X-ray energy spectrum (SEM-EDS) once again confirmed the successful fabrication of Ag<sub>2</sub>S since the atomic proportion of Ag and S is approximately 2:1 in the element distribution of the synthetic materials, taking the reaction for 10 min as an example (Riojas et al., 2019; Wong et al., 2022).

In order to analyze the morphology and crystal phase of the composite, the transmission electron microscopy (TEM) was carried out and the results are shown in Fig. 1. Fig. 1a-c exhibits that the generated Ag<sub>2</sub>S nanoparticles in every group have uniform particle size and good dispersibility. Moreover, with the prolonging of the reaction time, the average size of Ag<sub>2</sub>S nanoparticles kept increasing with the diameter ranging from ~ 10 nm to ~ 30 nm. From the TEM images of Ag<sub>2</sub>S/RGO as illustrated in Fig. 1d, it can be seen that the Ag<sub>2</sub>S was round and successfully attached to the RGO surface, and the agglomeration of the nanomaterials was effectively prevented. Moreover, the spherical morphology of silver sulfide increased the specific surface area of the composite material, which led to the enhancement of the light absorption ability. Therefore, the photocatalytic activity of the composites was improved (Shafi et al., 2019). Besides, the inset histogram for the particle size distribution in Fig. 1d also demonstrated the major diameter of ~ 10 nm. To further confirm the structure of the fabricated materials, high resolution TEM studies were performed as depicted in Fig. 1e. After comparing with the standard cards, it can be determined to be (111) crystal surface and the lattice spacing is 0.2836 nm (Chih and Yang 2014), which is consistent with monoclinic crystal system. These results confirm that the observed nanocrystals on the RGO layer are Ag<sub>2</sub>S

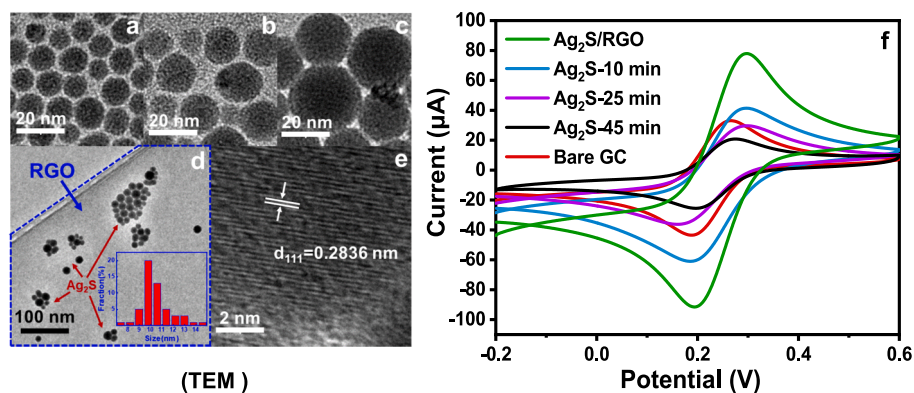


**Fig. 1.** TEM images of Ag<sub>2</sub>S nanoparticles with (a) 10 min reaction time, (b) 25 min reaction time, and (c) 45 min reaction time; (d) TEM images of Ag<sub>2</sub>S/RGO materials at 10 min reaction time with inset of the histogram for the particle size distribution; (e) HR-TEM images of Ag<sub>2</sub>S nanoparticles on the RGO; (f) CV plots of bare GCE, Ag<sub>2</sub>S/RGO/GCE and Ag<sub>2</sub>S/GCE in 20 mmol·L<sup>-1</sup> [Fe(CN)<sub>6</sub>]<sup>3-/4-</sup> solution.

nanoparticles with a uniform spherical structure.

Fig. 1f displays the electrochemical cyclic voltammetry (CV) of Ag<sub>2</sub>S and Ag<sub>2</sub>S/RGO modified electrodes in 0.1 mol L<sup>-1</sup> KCl solution of 20 mmol L<sup>-1</sup> [Fe(CN)<sub>6</sub>]<sup>3-/4-</sup>. Firstly, although the current intensity of Fe<sup>2+</sup>/Fe<sup>3+</sup> on Ag<sub>2</sub>S/GCE has no obvious advantage compared with that on the bare electrode, the current response with the reaction time of 10 min is the largest and the redox peak potential difference decreases, which proves that Ag<sub>2</sub>S has good electrocatalytic performance and increases the reversibility of the electrochemical reaction. For Ag<sub>2</sub>S modified systems, it can be seen from Fig. 1f that the Fe<sup>2+</sup>/Fe<sup>3+</sup> redox peak current increased on Ag<sub>2</sub>S modified electrode (Ag<sub>2</sub>S/GCE) with the shorter reaction time. The results can be explained that the smaller the size of nanoparticles, the larger the specific surface area, and the faster the electron transfer. In order to further improve the electrochemical properties of modified electrode and the potential response to gatifloxacin, the Ag<sub>2</sub>S/RGO modified electrode (Ag<sub>2</sub>S/RGO/GCE) was constructed (10 min reaction time). Fig. 1f shows that the peak current of Fe<sup>2+</sup>/Fe<sup>3+</sup> on the Ag<sub>2</sub>S/RGO/GCE is the largest. The combination of silver sulfide and RGO effectively prevents the agglomeration of nanomaterials and increases the specific surface area of the composite due to the Ag<sub>2</sub>S nanoparticles, thus enhancing the photocatalytic activity. The observed higher current at Ag<sub>2</sub>S/RGO composites and the synergistically enhanced electrochemical properties might speculatively be attributed to the following three aspects: (i) the abundant oxygen-containing groups and high adsorption capacity of RGO might do favor to the touching of targeted GAT to the modified electrode; (ii) the large specific surface area of Ag<sub>2</sub>S nanoparticles might provide more abundant active sites for the GAT reaction; and (iii) the Ag<sub>2</sub>S/RGO composites may further improve the good conductivity of the electrode material as mentioned above.

Electrochemical impedance spectroscopy (EIS) can provide useful information regarding impedance changes on the electrode surface during the fabrication process. The charge-transfer resistance was related to the electron-transfer kinetics of the redox probe ([Fe(CN)<sub>6</sub>]<sup>3-/4-</sup>) at the electrode interface and could be estimated from the diameter of the semicircular part of the EIS curve. The typical Nyquist plots obtained from bare GC, Ag<sub>2</sub>S/GC, RGO/GC, and Ag<sub>2</sub>S/RGO/GC (with RCT values of about 360, 440, 290, 60, respectively) in aqueous KCl (0.1 mol/L) containing 20 mmol/L [Fe(CN)<sub>6</sub>]<sup>3-/4-</sup> were illustrated in Fig. S6. A large diameter of the semicircle part was observed for GC. The diameter of the semicircle was increased when the GC surface was coated with Ag<sub>2</sub>S nanoparticles due to poor electrical conductivity. The semicircle diameter showed the decrease in RGO/GC due to the excellent electron transfer ability. The electrochemical impedance spectrum of Ag<sub>2</sub>S/RGO/GC had the smallest semicircle diameter, which proved that the fastest electron-transfer kinetics of [Fe(CN)<sub>6</sub>]<sup>3-/4-</sup> occurred in Ag<sub>2</sub>S/RGO/GC rather than in other modified electrodes. So the EIS results were in full

agreement with the CV results. These results generally indicate that Ag<sub>2</sub>S/RGO has good electrocatalytic ability and extremely strong conductivity, which can provide strong support for the subsequent detection of gatifloxacin.

### 3.2. Optimization of Ag<sub>2</sub>S/RGO/GCE based electrochemical sensor

Fig. 2a illustrated the LSV curves of 200 µmol·L<sup>-1</sup> gatifloxacin on bare GCE and Ag<sub>2</sub>S/RGO/GCE with a sweep rate of 0.1 V·s<sup>-1</sup>. It can be observed that I<sub>pa</sub> of gatifloxacin on Ag<sub>2</sub>S/RGO/GCE is significantly increased, which is about 2.5 times of that on the bare electrode. It turns out that Ag<sub>2</sub>S/RGO with large specific surface area and good conductivity has a good catalytic effect on the electrochemical oxidation of gatifloxacin and accelerates the electron transfer on the electrode. Thus, the Ag<sub>2</sub>S/RGO modified GCE was used in designing the electrochemical sensors for gatifloxacin detection. As reported before, the electrochemical reaction of GAT has been reported to be a two electron-transferred oxidation process accompanied by two proton releasing due to GAT's redox mechanistic properties (Li et al., 2024; Zhu et al., 2020). Thus, the mechanism herein may possibly be the addition of hydroxyl group on the N4 atom with the formation of a hydroxylamine during electro-oxidation, which is a process of two electron transfer and two proton loss, similar to previous publications (Li et al., 2024; Zhu et al., 2020). To make it clear, the speculative reaction equation was depicted in Scheme 1 with the possible electron transfer process and the potential reaction product.

Fig. 2b displays the cyclic voltammogram (CV) profiles of 200 µmol/L gatifloxacin at the bare glassy carbon electrode and the Ag<sub>2</sub>S/RGO/GCE with a sweep rate of 0.1 V·s<sup>-1</sup>. The electrochemical oxidation of gatifloxacin at the Ag<sub>2</sub>S/RGO/GCE shows a significant increase of about 2.5-fold compared to the bare electrode, along with a negative shift of the peak potential (-0.01 V). This suggests that Ag<sub>2</sub>S/RGO/GCE, with its large specific surface area and good conductivity, has a positive catalytic effect and accelerates electron transfer on the electrode.

Apart from that, Fig. S3 in the Supplementary Materials illustrated the linear sweep voltammetry (LSV) curves of the bare GCE and Ag<sub>2</sub>S/GCE prepared at different reaction times in gatifloxacin solution of 200 µmol·L<sup>-1</sup>, with a scanning rate of 0.1 V/s. It was observed that the oxidation peak potential is near 1.1 V, and the electrochemical response of gatifloxacin on Ag<sub>2</sub>S/GCE was slightly different with different reaction time. As mentioned before, different reaction time will affect the size of Ag<sub>2</sub>S nanoparticles. The results show that the shorter the reaction time is, the smaller the grain size is, and the better electrochemical signal is. Sheng et al. (2014) reported a monocryalline 3D TiO<sub>2</sub> branching nanowire array consisting of one-dimensional branching that grows epitaxial from the backbone. The 3D branched-chain nanoarrays exhibited an increase in the specific surface area, along with

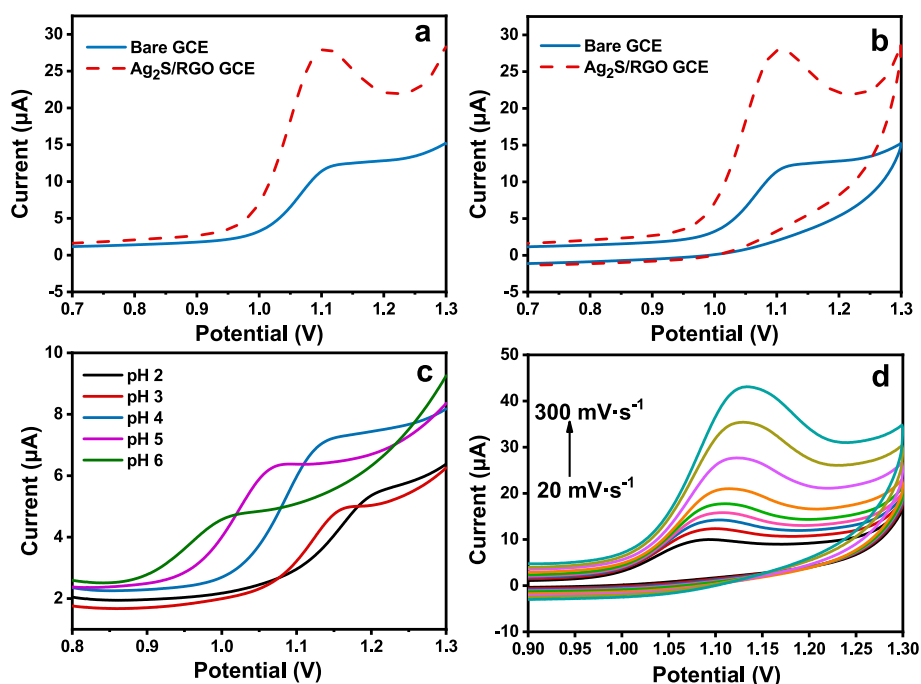


**Fig. 2.** (a) LSV plots of Ag<sub>2</sub>S/RGO/GCE and bare GCE in 200 μmol·L<sup>-1</sup> gatifloxacin solution; (b) CV plots of bare GCE and Ag<sub>2</sub>S/RGO/GCE in 200 μmol·L<sup>-1</sup> gatifloxacin solution; (c) LSV of 40 μmol·L<sup>-1</sup> gatifloxacin at Ag<sub>2</sub>S/RGO/GCE electrode in the different buffer solution with various pH values; (d) Cyclic voltammograms of Ag<sub>2</sub>S/RGO/GCE electrode at different scan rates in 100 μmol·L<sup>-1</sup> gatifloxacin solution.

characteristics of rapid charge transfer and high absorption capacity (Sheng et al., 2014). Therefore, the probable reason might be that the specific surface area is larger and the electron transfer is faster for the small-size Ag<sub>2</sub>S nanoparticles, which consequently result in the better electrochemical performance. Therefore, the Ag<sub>2</sub>S with the shortest reaction time (10 min) and the smallest particle size is selected as the initial modified electrode material. Due to the imino group of gatifloxacin molecules, pH in PBS buffer solution might affect the electrochemical response of gatifloxacin. Fig. 2c shows the LSV response of gatifloxacin on Ag<sub>2</sub>S/RGO electrode in PBS solution with different pH values. pH variations in PBS buffer solution will affect the electrochemical response of gatifloxacin. We could observe that with the increase of pH, *I*<sub>pa</sub> firstly increased and then began to decrease. It can be concluded that the best pH of PBS solution is 4 for the electrolyte. Moreover, with the decrease of pH, the oxidation peak potential of gatifloxacin at Ag<sub>2</sub>S/RGO electrode was found negatively shifted. It exhibited a linear relationship between the potential and pH, as shown in Fig. S4, with the linear regression equation of  $E_{pa}(V) = -0.047pH + 1.300$  ( $R^2 = 0.9886$ ). This tendency indicated the protons participate in the oxidation of gatifloxacin. The slope in this relationship ( $-47$  mV/pH) approximated the theoretical value of  $-59$  mV/pH (Jiang et al. 2016; Zhang et al., 2013b; Li et al., 2024; Zhu et al., 2020). This indicated that the proton number and electron transfer number involved in the oxidation of gatifloxacin on Ag<sub>2</sub>S/RGO electrodes were equal, implying that it possibly followed the 2-electron-2-proton mechanism (Jiang et al. 2016; Zhang et al., 2013b; Li et al., 2024; Zhu et al., 2020). Generally, the current result was in accordance with the reported value and the probable mechanism of the reaction was surmised as shown in Scheme 1.

Scanning rate is of great importance for the sensing performance of an electrochemical sensor, so the effect of scanning rate on the electrochemical current response was also investigated next. As shown in Fig. 2d, when the scanning rate increases gradually from 20 mV·s<sup>-1</sup> to 300 mV·s<sup>-1</sup>, *I*<sub>pa</sub> of GAT kept increasing with the *E*<sub>pa</sub> moving forward gradually. The results suggested that the current reaction is an electrochemical process controlled by adsorption of GAT on Ag<sub>2</sub>S/RGO electrode and the oxidation reaction of GAT is irreversible in this process. It

is worth noting that *I*<sub>pa</sub> of GAT decreased with the decrease of *v*, and thus, the sensitivity could also be weakened. Meanwhile, with the increase of *v*, *I*<sub>pa</sub> also increased, but *E*<sub>pa</sub> shifted positively. Therefore, it is necessary to select the relatively optimal scanning rate on consideration of both the current response and the sensitivity. Finally, after comprehensive consideration, the optimized scanning rate was determined as 100 mV·s<sup>-1</sup> for the following electrochemical sensing tests.

### 3.3. Linear range and sensitivity

After the multiple optimization, Ag<sub>2</sub>S/RGO/GCE accomplished LSV detection of gatifloxacin under optimal experimental conditions (pH 4.0, *v* of 100 mV·s<sup>-1</sup>), and the working curve was obtain as shown in Fig. 3. Generally speaking, for both concentration range, the *I*<sub>pa</sub> continuously increased with the rise of gatifloxacin concentration in Fig. 3a and 3b. Furthermore, as shown in Fig. 3c and 3d, in the concentration range of 0.2 μmol·L<sup>-1</sup> ~ 20 μmol·L<sup>-1</sup> and 20 μmol·L<sup>-1</sup> ~ 250 μmol·L<sup>-1</sup>, there are good linear relationships between *I*<sub>pa</sub> and concentration of gatifloxacin on Ag<sub>2</sub>S/RGO/GCE. At low concentration, the linear regression equation is:  $I_{pa} (\mu A) = 0.07212c (\mu mol \cdot L^{-1}) + 0.0216$  ( $R^2 = 0.9947$ ). At high concentration, the linear regression equation is:  $I_{pa} (\mu A) = 0.0973c (\mu mol \cdot L^{-1}) - 1.6688$  ( $R^2 = 0.9983$ ). The detection limit was calculated to be  $6.67 \times 10^{-8}$  mol·L<sup>-1</sup> base on the formula of Signal/Noise being 3:1 (Liu et al., 2021).

In order to evaluate the detection performance of the constructed sensors more intuitively, we compared this study with the existing literatures about GAT sensors as listed in Table 1. In general, the proposed Ag<sub>2</sub>S/RGO-based sensor shows relatively wide linear ranges for both low and high concentrations of GAT. This performance is, to some extent, at leading level among the existing GAT sensors whose linear ranges are often located at either low or high concentrations as shown in Table 1. Moreover, the limit of detection (LOD) of this sensor is relatively low (0.0667 μmol·L<sup>-1</sup>), justifying the high sensitivity and remarkable advantage of the currently proposed sensor.

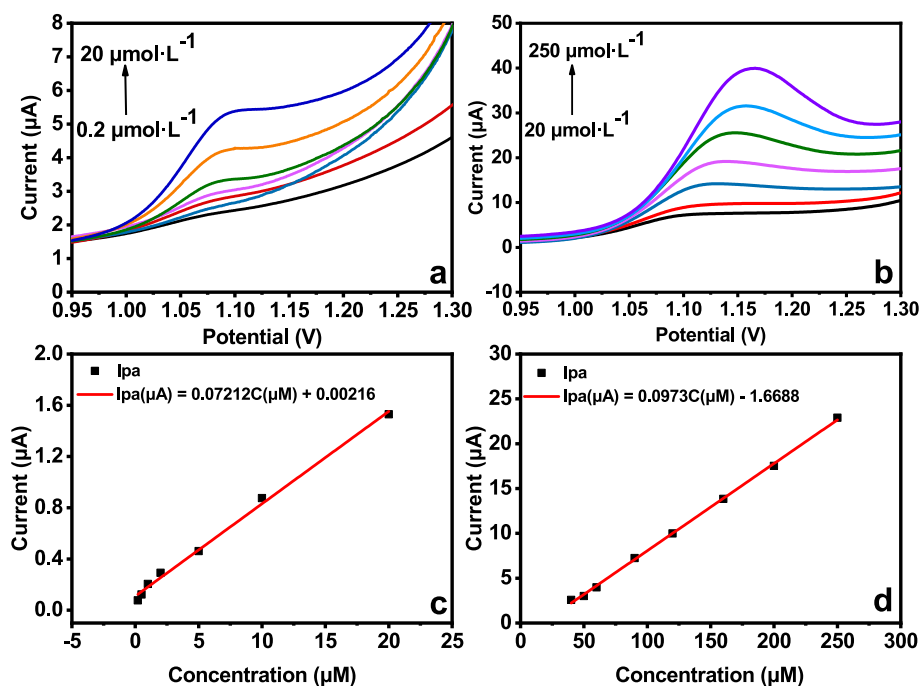


Fig. 3. LSV of different concentrations of gatifloxacin at  $\text{Ag}_2\text{S}/\text{RGO}/\text{GCE}$ : (a)  $0.2 \mu\text{mol}/\text{L} - 20 \mu\text{mol}/\text{L}$ , (b)  $20 \mu\text{mol}/\text{L} - 250 \mu\text{mol}/\text{L}$ ; Calibration curves of the concentration and oxidation current of gatifloxacin: (c)  $0.2 \mu\text{mol}/\text{L} - 20 \mu\text{mol}/\text{L}$ , (d)  $20 \mu\text{mol}/\text{L} - 250 \mu\text{mol}/\text{L}$ .

Table 1

Comparison of the  $\text{Ag}_2\text{S}/\text{RGO}/\text{GCE}$  in Sensing GAT with the Existing Electrochemical Sensors.

Electrodes	Methods	Linear ranges ( $\mu\text{mol}\cdot\text{L}^{-1}$ )	LODs ( $\mu\text{mol}\cdot\text{L}^{-1}$ )	Sensitivity ( $\mu\text{A} \mu\text{M}^{-1}$ )	References
$\beta$ -cyclodextrin/rGO/GCE	Differential Pulse Voltammetry (DPV)	0.05 ~ 150	0.02	0.33	(Jiang et al., 2016)
Multi-walled carbon nanotubes-polymeric alizarin	Linear Sweep Voltammetry (LSV)	5 ~ 100	0.4	0.267	(Chi and Li, 2010)
zirconium-based metal-organic framework-carboxylated multiwalled nanotube nanocomposites	Linear Sweep Voltammetry (LSV)	0.05 ~ 10	0.0075	5.2	(Wan et al., 2023)
P-L CuO: $\text{Tb}^{3+}$ NS/GCE	Differential Pulse Voltammetry (DPV)	0.1 ~ 800	0.0012	0.072	(Taherizadeh et al., 2023)
Cysteic acid/CPE	Differential Pulse Voltammetry (DPV)	0.02 ~ 200	0.01	0.79	(Zhang et al., 2013a)
Cetyltrimethylammonium bromide/Cu-graphene nanoparticle/CPE	Differential Pulse Voltammetry (DPV)	0.02 ~ 40	0.0021	0.031	(Zhu et al., 2020)
DNA/GCE	Differential Pulse Voltammetry (DPV)	0.2 ~ 1.4	0.05	0.186	(Radi et al., 2010)
P- $\beta$ -cyclodextrin-L-arg/CPE	Differential Pulse Voltammetry (DPV)	0.06 ~ 100	0.02	0.25	(Zhang et al., 2013b)
ssDNA/single wall carbon nanotube	Square Wave Voltammetry (SWV)	1 ~ 10	0.752	0.11	(Moraes et al., 2013)
$\text{Ag}_2\text{S}/\text{RGO}/\text{GCE}$	LSV	0.2 ~ 20; 20 ~ 250	0.0667	0.072; 0.097	This study

### 3.4. Repeatability, reproducibility, and selectivity

Repeatability and reproducibility are two essential indexes for a sensor. Therefore, the same  $\text{Ag}_2\text{S}/\text{RGO}/\text{GCE}$  was constructed for five times in the same concentration of gatifloxacin solution and the relative standard deviation (RSD) was calculated to be 1.9%. Furthermore, five  $\text{Ag}_2\text{S}/\text{RGO}/\text{GCE}$  with the same conditions were prepared and tested in the same gatifloxacin solution with a RSD of 3.5%. The bar diagram for the repeatability and reproducibility of the sensor was illustrated in Fig. S5. These results show that the fabricated  $\text{Ag}_2\text{S}/\text{RGO}/\text{GCE}$  sensor has good repeatability and reproducibility. Moreover, the long-term stability of the sensor is also an important factor which deserves consideration. The results show that after storage for one week at room temperature, the same sensor retained a current response of 97.5% of

the initial current, indicating the satisfactory stability of the developed electrochemical sensor.

Besides, in the actual environments, the sensing platforms are often co-existed with various probable interferences, so the interference resistance of the proposed sensors should be investigated. Herein, we investigated the influence of various possible interferences through mixing  $40 \mu\text{mol}\cdot\text{L}^{-1}$  of different compounds, including ions, organic compounds, and other antibiotics (ciprofloxacin (CIP), enoxacin (ENX), norfloxacin (NFO), ascorbic acid (ASA), glucose (GLC), levodopa (L-dopa), uric acid (UA),  $\text{K}^+$ ,  $\text{Mg}^{2+}$ ,  $\text{Fe}^{3+}$ ,  $\text{Zn}^{2+}$ ) with  $40 \mu\text{mol}\cdot\text{L}^{-1}$  GAT in the acetate buffer solution (pH = 4). As depicted in Fig. 4, none of the tested interferences interfered the accurate analysis of GAT, suggesting that the proposed GAT sensors in this study possess high selectivity and anti-interference. Overall, this electrochemical sensor based on  $\text{Ag}_2\text{S}/\text{RGO}/$

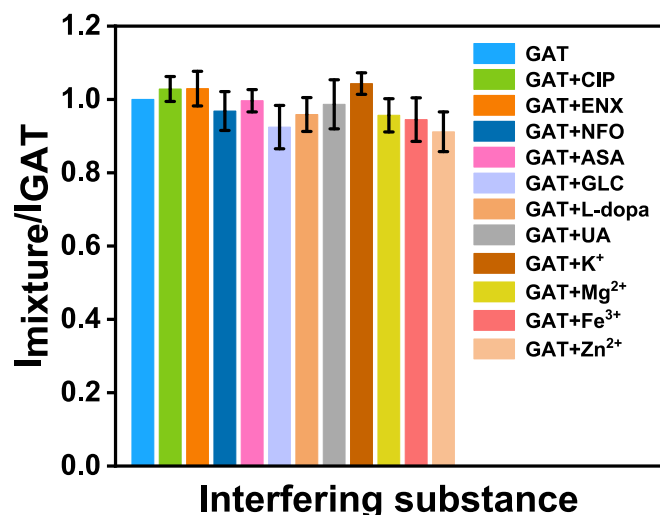


Fig. 4. Response of the  $\text{Ag}_2\text{S}/\text{RGO}/\text{GCE}$  sensor to GAT with or without interfering substances.

GCE has good selectivity, low detection limit, and wide range of linearity, for the sensing of GAT, and exhibits promising potential in the analysis of GAT in real samples.

### 3.5. Real sample analysis

In order to verify the applicability of  $\text{Ag}_2\text{S}/\text{RGO}/\text{GCE}$  sensor in real samples, the standard addition method is utilized to test the detection performance in various real samples and the results are listed in Table 2. It can be seen that the recovery rates are within the range of 91.8 % – 102.4 % after the addition of various GAT concentrations, suggesting that the proposed electrochemical sensor is effective and reliable for the gatifloxacin analysis in different real samples. Moreover, all the RSDs were lower than 4.0 % after 5 repetitions, revealing the excellent precision and stability of the developed sensors.

## 4. Conclusion

In this work, a novel  $\text{Ag}_2\text{S}/\text{RGO}$  composite with good conductivity and large specific surface area was synthesized and applied in the fabrication of an electrochemical sensor for GAT. After optimization of the electrochemical properties, the developed  $\text{Ag}_2\text{S}/\text{RGO}$  electrochemical sensing platform show accurate and efficient analytical performance for GAT with high sensitivity, good reproducibility and repeatability, high selectivity, and satisfactory stability. More importantly, the fabricated sensors were successfully applied in the GAT analysis in various real samples (including stern, crucian carp, and chicken meat) with satisfactory recoveries, indicating its practically applicable capacity for GAT analysis. Potentially, the definite sensing mechanism should be further explored in future works. In general, the current work provides a new avenue for the effective detection of GAT antibiotics, which is helpful for accurately assess the occurrence of antibiotics in the environment and can also give instructive insight into the development of sensing or analytical techniques through the fabrication of various functional materials.

### CRedit authorship contribution statement

**Chunxia Yao:** Writing – original draft, Validation, Methodology, Conceptualization. **Ying Liang:** Writing – original draft, Validation, Methodology, Investigation, Data curation. **Sai Huang:** Writing – review & editing, Validation, Investigation. **Chengbin Liu:** Writing – review & editing, Project administration, Methodology, Funding acquisition,

Table 2

Detection Results for GAT in Various Real Samples (n = 4).

Sample	Spiked Concentration ( $\mu\text{mol}\cdot\text{L}^{-1}$ )	Mean value ( $\mu\text{mol}\cdot\text{L}^{-1}$ )	Recovery (%)	RSD (%)
Stern	10	9.18	91.8	2.76
	100	93.41	93.4	3.17
	200	190.83	95.4	2.34
Crucian carp	10	9.23	92.3	2.52
	100	96.18	96.2	2.26
	200	196.56	98.3	2.31
Chicken meat	10	9.46	94.6	2.98
	100	96.83	96.8	3.34
	200	204.74	102.4	2.49

Formal analysis, Conceptualization. **Wei Song:** Writing – review & editing, Validation, Funding acquisition. **Weiguo Song:** Writing – review & editing, Validation, Funding acquisition.

### Declaration of Competing Interest

The authors declare that they have no known competing financial interests or personal relationships that could have appeared to influence the work reported in this paper.

### Acknowledgements

This work was supported by the Foundation of Shanghai Municipal Commission of Science & Technology Commission (21 N51900600), the Shanghai Rising-Star Program (23QB1403400), the Program of Shanghai Technology Research Leader (23XD1432900), and the Outstanding team of Shanghai Academy of Agricultural Sciences (2022-010).

### Appendix A. Supplementary data

Supplementary data to this article can be found online at <https://doi.org/10.1016/j.arabjc.2024.106031>.

### References

- Abd El-Rahman, M.K., Sayed, R.A., El-Masry, M.S., et al., 2021. A Novel in Situ Electrochemical Strategy for Gatifloxacin Microdetermination in Urine Using Solid Contact and Disposal Screen-Printed Electrodes: a Comparative Study. *Janal. Chem.* 76, 243–251. <https://doi.org/10.1134/S1061934821020064>.
- Akkarachanchainon, N., Rattanawaleedirojn, P., Chailapakul, O., et al., 2017. Hydrophilic graphene surface prepared by electrochemically reduced micellar graphene oxide as a platform for electrochemical sensor. *Talanta* 165, 692–701. <https://doi.org/10.1016/j.talanta.2016.12.092>.
- Aydin, B.Ş., Keziban, A., Nuray, G., 2024. Green synthesis of  $\text{Ag}_2\text{S}$  nanoparticle from sweet cherry on ultrasound-assisted prepared  $\text{NiMoO}_4/\text{g-C}_3\text{N}_4$  nanocomposite for photocatalytic  $\text{H}_2$  production. *J. Alloys Comp.* 976 (5), 172996. <https://doi.org/10.1016/j.jallcom.2023.172996>.
- Bo, X., Zhou, M., Guo, L., 2017. Electrochemical sensors and biosensors based on less aggregated graphene. *Biosens. Bioelectron.* 89, 167–186. <https://doi.org/10.1016/j.bios.2016.05.002>.
- Cai, M., Ding, C., Wang, F., et al., 2019. A ratiometric fluorescent assay for the detection of alkaline phosphatase based on near infrared  $\text{Ag}_2\text{S}$  quantum dots and calcein. *Biosens. Bioelectron.* 137, 148–153. <https://doi.org/10.1016/j.bios.2019.04.057>.
- Chekin, F., Bagga, K., Subramanian, P., et al., 2018. Nucleic aptamer modified porous reduced graphene oxide/ $\text{MoS}_2$  based electrodes for viral detection: Application to human papillomavirus (HPV). *Sensor. Actuat. B-Chem.* 262, 991–1000. <https://doi.org/10.1016/j.snb.2018.02.065>.
- Chekin, F., Myshin, V., Ye, R., et al., 2019. Graphene-modified electrodes for sensing doxorubicin hydrochloride in human plasma. *Anal. Bioanal. Chem.* 411 (8), 1509–1516. <https://doi.org/10.1007/s00216-019-01611-w>.
- Chen, Y.C., Bai, Y.M., Hsu, Y.K., 2021. Biomarker detection for disease diagnosis via versatile  $\text{Ag}_2\text{S}$  nanowires as electrochemical sensor and SERS substrate. *J. Alloy. Compd.* 881, 160647. <https://doi.org/10.1016/j.jallcom.2021.160647>.
- Chen, H., Li, B., Zhang, M., et al., 2014. Characterization of tumor-targeting  $\text{Ag}_2\text{S}$  quantum dots for cancer imaging and therapy in vivo. *Nanoscale* 6 (21), 12580–12590. <https://doi.org/10.1039/C4NR03613A>.
- Chi, Y., Li, J., 2010. Determination of levofloxacin hydrochloride with multiwalled carbon nanotubes-polymeric alizarin film modified electrode. *Russ. J. Electrochem.* 46, 155–160. <https://doi.org/10.1134/S1023193510020059>.

- Chih, Y.K., Yang, M.C., 2014. Simultaneous detection of dopamine and ascorbic acid using silver/silver sulfide modified carbon nanotube electrodes. *J. Taiwan. Inst. Chem. e.* 45 (3), 833–839. <https://doi.org/10.1016/j.jtice.2013.09.005>.
- Darwish, I.A., Sultan, M.A., Al-Arfaj, H.A., 2010. Selective kinetic spectrophotometric method for determination of gatifloxacin based on formation of its N-vinyl chlorobenzoquinone derivative. *Spectrochim. Acta. a.* 75, 334–339. <https://doi.org/10.1016/j.saa.2009.10.036>.
- Du, Y.P., Xu, B., Fu, T., et al., 2010. Near-Infrared Photoluminescent Ag<sub>2</sub>S Quantum Dots from a Single Source Precursor. *J. Am. Chem. Soc.* 132 (5), 1470–1471. <https://doi.org/10.1021/ja909490r>.
- Ghayeb, Y., Momeni, M.M., Mozafari, A., 2016. Effect of silver sulfide decorating on structural, optical and photo catalytic properties of iron-doped titanium dioxide nanotubes films. *J. Mater. Sci-Mater. El.* 27, 11804–11813. <https://doi.org/10.1007/s10854-016-5321-8>.
- Huang, Y., Sun, X., Yang, J., et al., 2023. A molecularly imprinted electrochemical sensor with dual functional monomers for selective determination of gatifloxacin. *Microchim. Acta* 190, 261. <https://doi.org/10.1007/s00604-023-05839-3>.
- Jang, A.R., Lim, J.E., Jang, S., et al., 2021. Ag<sub>2</sub>S nanoparticles decorated graphene as a selective chemical sensor for acetone working at room temperature. *Appl. Surf. Sci.* 562, 150201. <https://doi.org/10.1016/j.apsusc.2021.150201>.
- Ji, Y., Bai, X., Tang, J., et al., 2024. Photocathodic Activation of Peroxymonosulfate in a Photofuel Cell: A Synergistic Signal Amplification Strategy for a Self-Powered Photoelectrochemical Sensor. *Anal. Chem.* 96, 3470–3479. <https://doi.org/10.1021/acs.analchem.3c05098>.
- Jiang, Z., Li, G., Zhang, M., 2016. Electrochemical sensor based on electropolymerization of  $\beta$ -cyclodextrin and reduced-graphene oxide on glassy carbon electrode for determination of gatifloxacin. *Sens. Actu. B-Chem.* 228, 59–65. <https://doi.org/10.1016/j.snb.2016.01.013>.
- Kang, K., Xie, S., Huang, L., et al., 2015. High-mobility three-atom-thick semiconducting films with wafer-scale homogeneity. *Nature* 520, 656–660. <https://doi.org/10.1038/nature14417>.
- Karuppasamy, P., Karthika, A., Senthilkumar, S., et al., 2022. An Efficient and Highly Sensitive Amperometric Quercetin Sensor Based on a Lotus Flower Like SeO<sub>2</sub>-Decorated rGO Nanocomposite Modified Glassy Carbon Electrode. *Electrocatalysis* 13, 269–282. <https://doi.org/10.1007/s12678-022-00707-9>.
- Keziban, A., 2019. CuFe<sub>2</sub>O<sub>4</sub>/reduced graphene oxide nanocomposite decorated with gold nanoparticles as a new electrochemical sensor material for L-cysteine detection. *J. Alloys Comp.* 791 (30), 391–401. <https://doi.org/10.1016/j.jallcom.2019.03.303>.
- Keziban, A., Nuray, G., Azize, A., et al., 2023. Novel green synthesis of Ag<sub>2</sub>S from Diospyros kaki and its application for efficient photocatalytic hydrogen evolution. *Mol. Catal.* 544 (15), 113140. <https://doi.org/10.1016/j.mcat.2023.113140>.
- Khadija, V., Salih, Z.B., Keziban, A., et al., 2023. A new sensing platform based on a ternary nanocomposite of graphitic carbon nitride–silver sulfide–nickel molybdate for quercetin determination. *Analyst* 148, 2159–2169. <https://doi.org/10.1039/D3AN00244F>.
- Ladmakhi, H.B., Chekin, F., Fathi, S., et al., 2020. Electrochemical sensor based on magnetite graphene oxide/ordered mesoporous carbon hybrid to detection of allopurinol in clinical samples. *Talanta* 211, 120759. <https://doi.org/10.1016/j.talanta.2020.120759>.
- Lahcen, A.A., Rauf, S., Beduk, T., et al., 2020. Electrochemical sensors and biosensors using laser-derived graphene: A comprehensive review. *Biosens. Bioelectron.* 168, 112565. <https://doi.org/10.1016/j.bios.2020.112565>.
- Li, X., Ma, Y., Zhong, X.L., et al., 2020. Silver sulfide nanoparticles on MWCNTs stabilized by poloxamer: An enhanced electrochemical sensor for high sensitivity detection of 2,4,6-trinitrotoluene. *Microchem. J.* 159, 105488. <https://doi.org/10.1016/j.microc.2020.105488>.
- Li, G., Wan, X., Zheng, Q., et al., 2024. Deep eutectic solvent-mediated synthesis of ZnCo<sub>2</sub>O<sub>4</sub>/MWCNT-COOH: Investigation of electrocatalytic activity for gatifloxacin detection. *Colloid. Surfaces A* 699, 134713. <https://doi.org/10.1016/j.colsurfa.2024.134713>.
- Liang, Y., Li, H., Hou, R., et al., 2019. Vertical stacking of copper sulfide nanoparticles and molybdenum sulfide nanosheets for enhanced nonlinear absorption. *ACS Appl. Mater. Interfaces.* 11, 35835–35844. <https://doi.org/10.1021/acsami.9b06662>.
- Liu, C., Wei, X., Hao, S., et al., 2021. Label-Free, Fast Response, and Simply Operated Silver Ion Detection with a Ti<sub>3</sub>C<sub>2</sub>T<sub>x</sub> MXene Field-Effect Transistor. *Anal. Chem.* 93 (22), 8010–8018. <https://doi.org/10.1021/acs.analchem.1c01094>.
- Lu, C., Chen, G., Yu, B., et al., 2018. Recent advances of low biological toxicity Ag<sub>2</sub>S QDs for biomedical application. *Adv. Eng. Mater.* 20 (6), 1700940. <https://doi.org/10.1002/adem.201700940>.
- Mao, K., Wu, D., Li, Y., et al., 2012. Label-free electrochemical immunosensor based on graphene/methylene blue nanocomposite. *Anal. Biochem.* 422 (1), 22–27. <https://doi.org/10.1016/j.ab.2011.12.047>.
- Mazurkó, J.M., Kusior, A., Mikula, A., et al., 2022. Transition metal sulfides for electrochemical applications: Controlled chemical conversion of CuS to Ag<sub>2</sub>S. *Appl. Surf. Sci.* 606, 154984. <https://doi.org/10.1016/j.apsusc.2022.154984>.
- Meng, Z., Shi, Z., Liang, S., et al., 2015. Residues investigation of fluoroquinolones and sulphenamides and their metabolites in bovine milk by quantification and confirmation using ultra-performance liquid chromatography-tandem mass spectrometry. *Food. Chem.* 174, 597–605. <https://doi.org/10.1016/j.foodchem.2014.11.067>.
- Mo, X., Zhu, C., Zhang, Z., et al., 2024. Nitrogen-Doped Indium Oxide Electrochemical Sensor for Stable and Selective NO<sub>2</sub> Detection. *Adv. Mater.* 2409294. <https://doi.org/10.1002/adma.202409294>.
- Moraes, F.C., Silva, T.A., Cesarino, I., et al., 2013. Antibiotic detection in urine using electrochemical sensors based on vertically aligned carbon nanotubes. *Electroanalysis* 25 (9), 2092–2099. <https://doi.org/10.1002/elan.201300261>.
- Neslihan, D., Keziban, A., Mustafa, O., et al., 2020. Design of a new electrochemical sensing system based on MoS<sub>2</sub>-TiO<sub>2</sub>/reduced graphene oxide nanocomposite for the detection of paracetamol. *New J. Chem.* 44, 11759–11767. <https://doi.org/10.1039/D0NJ02298E>.
- Radi, A.E., Wahdan, T., Anwar, Z., et al., 2010. Electrochemical and spectroscopic studies on the interaction of gatifloxacin, moxifloxacin and sparflaxacin with DNA and their analytical applications. *Electroanalysis* 22 (22), 2665–2671. <https://doi.org/10.1002/elan.201000285>.
- Riojas, A.A.C., Wong, A., Planes, G.A., et al., 2019. Development of a new electrochemical sensor based on silver sulfide nanoparticles and hierarchical porous carbon modified carbon paste electrode for determination of cyanide in river water samples. *Sens. Actu. B-Chem.* 287, 544–550. <https://doi.org/10.1016/j.snb.2019.02.053>.
- Santos, N.F., Pereira, S.O., Moreira, A., et al., 2021. IR and UV laser-induced graphene: application as dopamine electrochemical sensors. *Adv. Mater. Technol-Us.* 6 (6), 2100007. <https://doi.org/10.1002/admt.202100007>.
- Shafi, A., Ahmad, N., Sultana, S., et al., 2019. Ag<sub>2</sub>S-sensitized NiO-ZnO heterostructures with enhanced visible light photocatalytic activity and acetone sensing property. *ACS Omega* 4 (7), 12905–12918. <https://doi.org/10.1021/acsomega.9b01261>.
- Sheng, X., He, D., Yang, J., et al., 2014. Oriented assembled TiO<sub>2</sub> hierarchical nanowire arrays with fast electron transport properties. *Nano. Lett.* 14 (4), 1848–1852. <https://doi.org/10.1021/nl4046262>.
- Singh, M., Bhardiya, S.R., Rai, A., et al., 2023. Graphene-based nanomaterials for electrochemical sensing of hydrazine: a short review. *Curr. Anal. Chem.* 19 (1), 27–37. <https://doi.org/10.2174/1573411018666220421104413>.
- Speltini, A., Sturini, M., Maraschi, F., et al., 2015. Graphene-derivatized silica as an efficient solid-phase extraction sorbent for pre-concentration of fluoroquinolones from water followed by liquid-chromatography fluorescence detection. *J. Chromatogr. a.* 1379, 9–15. <https://doi.org/10.1016/j.chroma.2014.12.047>.
- Storey, J.M., Clark, S.B., Johnson, A.S., et al., 2014. Analysis of sulfonamides, trimethoprim, fluoroquinolones, quinolones, triphenylmethane dyes and methyltestosterone in fish and shrimp using liquid chromatography-mass spectrometry. *J. Chromatogr. b.* 972, 38–47. <https://doi.org/10.1016/j.jchromb.2014.09.009>.
- Taberzadeh, M., Jahani, S., Moradizadeh, M., et al., 2023. Synthesis of a dual-functional terbium doped copper oxide nanoflowers for high-efficient electrochemical sensing of ofloxacin, pefloxacin and gatifloxacin. *Talanta* 255, 124216. <https://doi.org/10.1016/j.talanta.2022.124216>.
- Tang, X., Zhou, Z., Zhou, L., et al., 2024. Acid-Triggered Degradation of Three-In-One Ag<sub>2</sub>S Quantum Dots for In Situ Ratiometric NIR-II Fluorescence Imaging-Guided Ion/Gas Combination Therapy. *Anal. Chem.* 96, 7687–7696. <https://doi.org/10.1021/acs.analchem.4c00619>.
- Thangavelu, K., Raja, N., Chen, S.M., et al., 2017. Nanomolar electrochemical detection of caffeic acid in fortified wine samples based on gold/palladium nanoparticles decorated graphene flakes. *J. Colloid. Interf. Sci.* 501, 77–85. <https://doi.org/10.1016/j.jcis.2017.04.042>.
- Tian, J., Hu, J., Yang, F., et al., 2014. Polyamidoamine dendrimers as off-column binding agent and in-column pseudostationary phase for efficient and sensitive capillary electrophoretic analysis of fluoroquinolones in chicken muscles. *Food. Chem.* 157, 498–503. <https://doi.org/10.1016/j.foodchem.2014.02.070>.
- Van Doorslaer, X., Dewulf, J., Van Langenhove, H., et al., 2014. Fluoroquinolone antibiotics: an emerging class of environmental micropollutants. *Sci. Total. Environ.* 500, 250–269. <https://doi.org/10.1016/j.scitotenv.2014.08.075>.
- Venkatesh, K., Muthukutty, B., Chen, S.M., et al., 2022. Spinel CoMn<sub>2</sub>O<sub>4</sub> nano-/micro-spheres embedded RGO nanosheets modified disposable electrode for the highly sensitive electrochemical detection of metol. *J. Ind. Eng. Chem.* 106, 287–296. <https://doi.org/10.1016/j.jiec.2021.11.005>.
- Vlassiok, I., Polizos, G., Cooper, R., et al., 2015. Strong and electrically conductive graphene-based composite fibers and laminates. *ACS Appl. Mater. Interfaces.* 7 (20), 10702–10709. <https://doi.org/10.1021/acsami.5b01367>.
- Vosough, M., Eshlaghi, S.N., Zadmand, R., 2015. On the performance of multiway methods for simultaneous quantification of two fluoroquinolones in urine samples by fluorescence spectroscopy and second-order calibration strategies. *Spectrochim. Acta. a.* 136, 618–624. <https://doi.org/10.1016/j.saa.2014.09.075>.
- Wan, X., Du, H., Tuo, D., et al., 2023. UiO-66/carboxylated multiwalled carbon nanotube composites for highly efficient and stable voltammetric sensors for gatifloxacin. *ACS Appl. Nano. Mater.* 6 (20), 19403–19413. <https://doi.org/10.1021/acsnan.3c03874>.
- Wang, L., Li, M., Li, B., et al., 2023. Electrochemical sensor based on laser-induced graphene for carbendazim detection in water. *Foods.* 12 (12), 2277. <https://doi.org/10.3390/foods12122277>.
- Wong, A., Santos, A.M., Cardenas-Riojas, A.A., et al., 2022. Voltammetric sensor based on glassy carbon electrode modified with hierarchical porous carbon, silver sulfide nanoparticles and fullerene for electrochemical monitoring of nitrite in food samples. *Food. Chem.* 383. <https://doi.org/10.1016/j.foodchem.2022.132384>.
- Wu, T., Alharbi, A., Kiani, R., et al., 2019. Quantitative principles for precise engineering of sensitivity in graphene electrochemical sensors. *Adv. Mater.* 31 (6), 1805752. <https://doi.org/10.1002/adma.201805752>.
- Wu, Q., Zhou, M., Li, Q.J., et al., 2018. Three-dimensional bandgap-tuned Ag<sub>2</sub>S quantum dots/reduced graphene oxide composites with enhanced adsorption and photocatalysis under visible light. *Catal. Sci. Technol.* 8, 5225–5235. <https://doi.org/10.1039/C8CY01522H>.
- Yao, C., Wang, H., Zhou, J., et al., 2024. Exploring a novel, sensitive, and efficient Pb<sup>2+</sup> electrochemical sensing strategy based on Cu-MOF. *Arab. J. Chem.* 17 (2), 105498. <https://doi.org/10.1016/j.arabjc.2023.105498>.

Zhang, F., Gu, S., Ding, Y., et al., 2013a. Simultaneous determination of ofloxacin and gatifloxacin on cysteic acid modified electrode in the presence of sodium dodecyl benzene sulfonate. *Bioelectrochemistry* 89, 42–49. <https://doi.org/10.1016/j.bioelechem.2012.08.008>.

Zhang, F., Gu, S., Ding, Y., et al., 2013b. A novel sensor based on electropolymerization of  $\beta$ -cyclodextrin and l-arginine on carbon paste electrode for determination of

fluoroquinolones. *Anal. Chim. Acta.* 770, 53–61. <https://doi.org/10.1016/j.aca.2013.01.052>.

Zhu, M., Li, R., Lai, M., et al., 2020. Copper nanoparticles incorporating a cationic surfactant-graphene modified carbon paste electrode for the simultaneous determination of gatifloxacin and pefloxacin. *J. Electroanal. Chem.* 857, 113730. <https://doi.org/10.1016/j.jelechem.2019.113730>.